

Article

Impact of Corrosion in Simulated Body Fluid on Fatigue Characteristics of 3D-Printed Polylactic Acid-Coated AM60 Magnesium Alloys

Seyed Ali Ashraf Talesh and Mohammad Azadi * 

Faculty of Mechanical Engineering, Semnan University, Semnan 35131-19111, Iran

* Correspondence: m_azadi@semnan.ac.ir

Abstract: In this research, the pure fatigue behaviors of AM60 magnesium alloy with polylactic acid (PLA) coating (PF-AM60-PLA) and the corrosion fatigue behaviors of magnesium alloy with PLA coating (CF-AM60-PLA) were evaluated. Polymer coating was made by fused deposition modeling (FDM) with a 3D printer and attached to standard fatigue test specimens with glue. Then, after 27 days of immersion in the simulated body fluid (SBF), the high-cycle bending fatigue test was performed on samples. Due to corrosion, the weight of the specimens was reduced by an average of 35%. The corrosion rate decreased in the first 7 days and then increased. PF samples with a coating had an average 49% increase in fatigue lifetime. Regarding the CF samples, despite the use of a 10-times stronger solution, the fatigue lifetime of these samples decreased by only 35%. The field-emission scanning electron microscopy (FESEM) results also showed cleavage plates and striations. In addition, the separation of the glue from the coating and Mg was observed. Corrosion products, in addition to microcracks and holes, were seen on the fracture surface of CF specimens, which caused the stress concentration and the crack initiation. Holes caused by the release of gases were also observed in polymer coatings, which were fabricated by 3D printing.

Keywords: high-cycle fatigue; AM60 magnesium alloy; polymer coating; fused deposition modeling; additive manufacturing; corrosion; simulated body fluid



Citation: Ashraf Talesh, S.A.; Azadi, M. Impact of Corrosion in Simulated Body Fluid on Fatigue Characteristics of 3D-Printed Polylactic Acid-Coated AM60 Magnesium Alloys. *Surfaces* **2024**, *7*, 88–107. <https://doi.org/10.3390/surfaces7010007>

Received: 22 December 2023

Revised: 14 January 2024

Accepted: 19 January 2024

Published: 5 February 2024



Copyright: © 2024 by the authors. Licensee MDPI, Basel, Switzerland. This article is an open access article distributed under the terms and conditions of the Creative Commons Attribution (CC BY) license (<https://creativecommons.org/licenses/by/4.0/>).

1. Introduction

AM60 magnesium alloys have perfect mechanical properties such as strength and high fracture toughness [1,2]. This material has a low density and is biocompatible. For this reason, AM60 was used in structures under corrosion and fatigue loads. Magnesium is used in many industries, such as automotive, aerospace, healthcare, and biomedical. Magnesium is also used in implants and stents [3–6].

Song et al. [7] searched for a comparison of the corrosion performance of AM60 magnesium alloys in an atmospheric environment, both with and without the application of self-healing coatings. The results indicated that rainwater in scratched areas can accelerate magnesium corrosion. Additionally, it was found that self-healing coatings possess better inhibitive properties. Liu et al. [8] explored the corrosion characteristics of the AM60 magnesium alloy that incorporated either cerium (Ce) or lanthanum (La) when subjected to thin electrolyte layers. The smart map analysis confirmed the skeletal structure formation from the rare earth (RE) alloying. Finally, the corrosion pattern observed in the AMRE1 alloy indicated the corrosion area, and the application of a thin electrolyte layer (TEL) effectively suppresses the development of pitting corrosion. Matsubara et al. [9] found the impact of iron impurity on the corrosion behaviors of AM60 and AM50 magnesium alloys. The findings suggested that an increase in the Fe/Mn ratio correlated with higher rates of corrosion. That article concluded that these inclusions had a role as initiation corrosion points. Xie et al. [10] researched enhancing the anti-corrosion and anti-wear characteristics of AM60 magnesium alloys. They improved this through ion implantation and a gradient

duplex coating. The research revealed a significant improvement in behavior under the corrosion condition of magnesium alloys when they were coated. This improvement was evident in the current density of corrosion. Kumar [11] researched the effects of incorporating hydroxyapatite (HA) into AZ91D, AJ62, and AM60 alloys. The study found that HA, through the formation of complex metal hydroxides, enhanced corrosion resistance. As a result, AJ62/3HA and AZ91D/3HA alloys were found to be promising bio-material candidates due to their finer grains, exceptional resistance to corrosion, and strong biocompatibility, making them suitable for various applications. Other studies were conducted on the corrosion behavior of the AM60 alloy in the NaCl environment. Researchers in these studies attempted to increase the strength under corrosion in the AM60 alloys by adding materials such as rare earth cerium and lanthanum metals, organic inhibitors, and mineral inhibitors [12–15].

Akbaripanah et al. [16] studied the impact of the equal channel angular pressing (ECAP) technique in addition to extrusion on the fatigue characteristics of the AM60 magnesium alloys. In the second pass of ECAP, researchers found that fatigue lifetime increased. This result was important because improvements were seen in both low-cycling and high-cycling. Khan et al. [17] investigated the fatigue behavior of anodized AM60 magnesium alloys when exposed to a humid environment. The researchers found that anodized samples under high humidity conditions (80% RH) slightly improved fatigue strength. Hiromoto et al. [18] conducted a study on the fatigue properties of bio-absorbable magnesium alloys with hydroxyapatite coatings, formed through the chemical solution deposition method. In the final phase of the research, the investigators discovered that the hydroxyapatite (HAp) coatings on the sample remained intact without developing cracks even after 10^7 fatigue cycles, considering the fatigue limit. This suggested that the HAp coating offered approximately 3% cyclic elongation, showcasing its potential to increase the durability of AZ31 magnesium alloy components in specific applications. Considering the wide range of applications for magnesium alloys, numerous studies have been carried out on these materials. As a result, a substantial body of research was dedicated to exploring the corrosion fatigue behaviors in magnesium alloys. Through these investigations, researchers sought to enhance the resistance of the alloy to corrosion fatigue by altering its composition and microstructure [19–25]. For example, Uematsu et al. [20] improved the corrosion fatigue strength of magnesium alloys with multilayer diamond-like carbon coatings. AlamKhan et al. [21] compared the corrosion fatigue behavior of die-cast and shot-blasted AM60 magnesium alloys. Ishihara et al. [22] investigated the corrosion fatigue resistance of an electrolytically plated magnesium alloy.

Shi et al. [26] investigated a novel MAO-PLA coating applied to zinc alloys with the potential for use as an orthopedic implant material. In the research, the Zn-0.5Mn-0.5Mg alloys were subjected to surface modification by micro-arc oxidation (MAO) in addition to sol-gel PLA techniques. This treatment enhanced osteogenesis and reduced material toxicity for potential medical applications. Ultimately, based on the results obtained, researchers concluded that the surface modification of the MAO-PLA on the Zn-0.5Mn-0.5Mg alloys appeared to be suitable for improving biocompatibility. Anand et al. [27] assessed bio-degradable composites, Zn-Mg-Mn-(HA), coated with a polymer-ceramic composite (PLA/HA/TiO₂) for orthopedic applications. They observed higher corrosion rates in the as-cast sample, 1Mg-1Mn-1HA, than 1Mg-1Mn. However, after applying the polymer-ceramic nanofiber composite coating, the corrosion rates significantly decreased in electrochemical tests. Wang et al. [28] investigated the corrosion resistance of biodegradable iron and zinc materials by applying a poly(lactic) acid (PLA) coating to these materials for temporary medical implant applications. The study found that PLA enhances the iron (Fe) corrosion rate more effectively than zinc (Zn). This observation is likely attributed to the non-passivating nature of iron in an acidic environment. Beyzavi et al. [29] explored bio-polymer coatings, generating these coatings on the AM60 magnesium alloy with 3D printing by fused deposition modeling (FDM) in their study. These coatings were applied to explore the electrochemical behavior of the treated magnesium alloys. Their data from the

electrochemical impedance spectroscopy revealed that the transparent polycaprolactone (PCL) and PLA coatings exhibited the highest impedance. However, all the biodegradable coatings exhibited a significant increase in impedance, approximately 63.1–99.7%, compared to the magnesium alloy.

Based on the conducted studies, it was determined that many researchers had worked in the field of AM60 corrosion, and their goal was to improve corrosion using various methods [7–15]. Moreover, studies have shown that the use of biodegradable polymer coatings such as PLA can have a positive impact on corrosion [26–29]. Furthermore, it was disclosed that several studies were carried out in the field of fatigue for AM60 alloys [16–25].

Therefore, the innovation of this research is to compare the fatigue lifetime of PLA-coated Mg after corrosion in the simulated body fluid (SBF) with uncoated Mg samples. In other words, one way to strengthen the magnesium alloys is through surface modification techniques. For this objective, after machining the initial AM60 samples, the 3D-printed PLA coating layers were added with glue to the gauge length of the specimen. Several samples were corroded in the SBF, and then fatigue testing was performed under bending loads. Finally, the fracture surface of the samples was evaluated in a microscopic state to find the damage mechanisms.

2. Materials and Methods

2.1. Materials and Manufacturing Method

The primary material used in the present research is a magnesium alloy. Then, the chemical composition of this alloy was determined using a quantitative test (based on a chemical analysis with the RMRC-WI-520-100-06 standard at the Razi Metallurgical Research Center, Tehran, Iran), and its results (the weight percentage of elements) are shown in Table 1. From the comparison of the obtained results with the ASTM B94 standard, it was concluded that the alloy used is AM60. Its field-emission scanning electron microscopy (FESEM) images and energy-dispersive X-ray spectroscopy (EDX) were used for the microscopic evaluations. The related data illustrated that the magnesium matrix is based on $Al_{12}Mg_{17}$, Al_6Mn , and MgO [30]. More details are provided in the study [30]. Standard fatigue test samples were made from this alloy by the casting method.

Table 1. The quantitative result for AM60 (wt.%).

	Mg	Mn	Zn	Si	Al	Ni	Cu
Bulk		0.3	0.07	0.04	5.5	0.004	0.01

After the production of standard fatigue test samples, polymer coatings were made separately using the fused deposition modeling (FDM) technique. The coating used in this research is polylactic acid (PLA). This polymer is biocompatible. Its melting temperature is 180–230 °C, and its density is 1240 kg/m³ [31,32]. The 3D printing parameters of these coatings are presented in Table 2. These parameters were chosen according to the literature [33,34].

Table 2. The 3D printing parameters.

Parameters	Speed (mm/s)	Nozzle Temperature (°C)	Bed Temperature (°C)	Infill in the First and Last Layer (%)	Infill in the Inner Layer (%)	Layer Height (µm)	Nozzle Diameter (mm)
Value	50	245	60	100	50	50	0.4

The polymer coatings were attached to magnesium fatigue standard samples using glue. In this research, epoxy glue from the Megapox 300 Ghafari brand was used. It was shown in the previous research [35] that epoxy adhesives were not harmful to humans. These adhesives are two components and are mixed together in equal proportions. For

bonding, the fatigue standard sample was first degreased with dishwashing liquid. Then, the adhesive was used between the surface of the base metal and the coating layers. Based on the instructions from the glue manufacturer, the samples were kept in room air for 24 h. Then, the tests were performed on samples. Figure 1 depicts the standard sample of fatigue testing, with and without coating.



Figure 1. The fatigue standard sample with and without coating before corrosion.

It was optically tried to use a uniform thickness of glue in the whole area of the gauge length of the sample (Figure 1). However, this issue was not measured and controlled, and therefore, it could be a root cause of the uncertainty. Since different samples were used for checking the repeatability of experiments under the same conditions, this issue could be ignored as a concern for affecting the fatigue lifetime. The quality and thickness of the glue were also evaluated by the field-emission scanning electron microscopy (FESEM) images from the fracture surface of the samples.

According to ASTM D4541, adhesion testing was conducted by the pull-off experiment. An adhesion device made by the Defelsko Company was used to perform this test. An adhesion test was performed on each sample at three different points. The average value and the standard deviation of the obtained results, which showed the amount of adhesion between the base metal and the coating, were measured at 4.29 ± 0.71 . In another study [36], the amount of adhesion between PLA and Mg, which were connected to each other by the electrolytic plasma oxidation method, was also measured. More details about these adhesion testing results can be found in the previous work [33].

2.2. Corrosion Test

Standard fatigue test samples with coatings were subjected to corrosion. For this purpose, the specimens were completely immersed in the $1\times$ simulated body fluid (SBF). But with time, no corrosion occurred. Figure 2 shows a corrosion fatigue standard sample with $1\times$ SBF after 30 days. In this image, as it can be seen, the coating layers were attached to the gauge length of the sample (after using glue on the base metal). Then, the other surfaces (the dumbbell-shaped parts) of the sample were also covered by the bee wax to prevent any corrosion of the base metal (where there were no coatings).

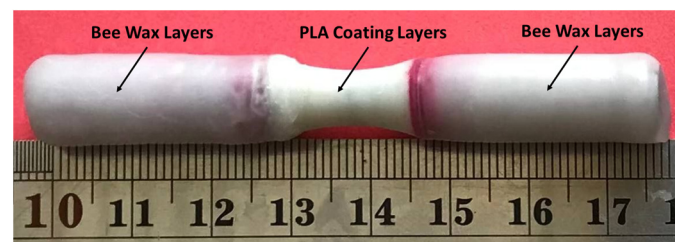


Figure 2. The corrosion fatigue standard sample with $1\times$ SBF after 30 days.

Then, to have higher corrosion rates, $10\times$ SBF was also used. The composition table of the SBF solution is depicted in Table 3. Based on this table, the main ions in the SBF solution are Na^+ and Cl^- . However, due to the presence of other ions, the corrosion effects with the NaCl solution will be completely different. For example, the hydrogen element can lead to the production of $\text{Mg}(\text{OH})_2$, which does not occur in the NaCl solution.

The samples were weighed every day for the first 7 days. Then, on days 13, 20, and 27, the weight of the specimens was recorded. It must be noted that before each weighing,

the samples were cleaned with a napkin and left in the open air for a few hours to dry completely. Figure 3 shows the fatigue standard sample with coatings after immersion in the SBF environment on different days. In addition, Figure 4 illustrates the specimen after corrosion testing, with and without corrosion products. As can be seen, in some cases, the coating layers were removed from the sample surface due to a high corrosion rate. Notably, all samples had complete coating layers on the gauge length. After the corrosion tests, in some specimens, a part of the coating layers was detached, and in others, the whole coating layers were detached from the surface. Therefore, the corrosion phenomenon could penetrate into the base metal, and a high corrosion rate occurred due to the low strength of AM60 magnesium alloys under the SBF condition or other mediums [7–15].

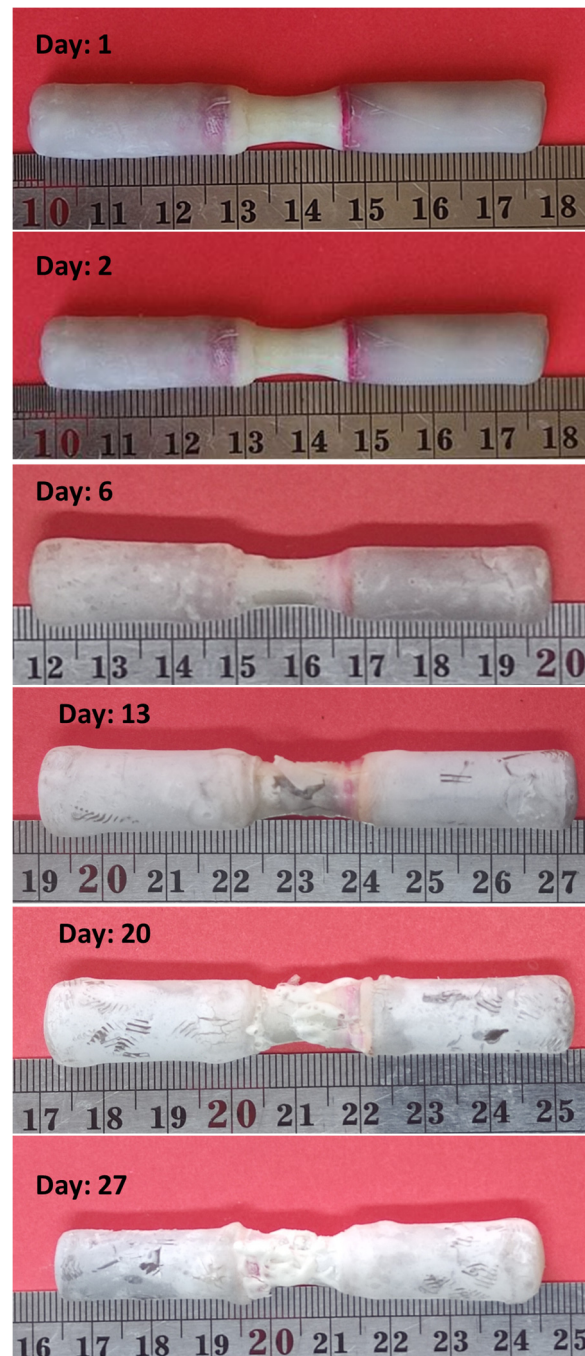


Figure 3. The image of standard samples during the corrosion test in 10× SBF.

Table 3. The constituent elements of the used SBF [37].

Ions	Concentration (mM)	Ions	Concentration (mM)
Mg ²⁺	15.0	HPO ₄ ²⁻	10.0
K ⁺	50.0	HCO ₃ ⁻	42.0
Na ⁺	1420.0	Cl ⁻	1478.0
Ca ²⁺	25.0	SO ₄ ²⁻	5.0

**Figure 4.** Samples after the corrosion test, with and without corrosion products.

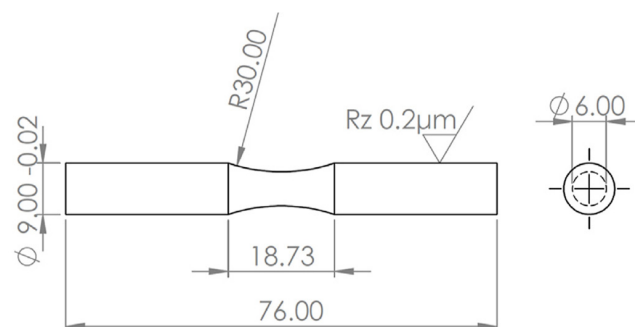
Based on the ASTM-G31-72 standard [38], the rate of corrosion can be calculated in mils per year (MPY) according to Equation (1), as follows:

$$\text{Corrosion rate} = \frac{KW}{AtD} \quad (1)$$

In this equation, A is the sample area (cm²), which is exposed to the environment, W is the weight loss (gr), D is the density of the material (gr/cm³), t is the exposure time (hr), and $K = 3.45 \times 10^6$ [38].

2.3. Fatigue Test

The high-cycle rotary bending fatigue test ($R = -1$) was performed based on the ISO-1143 and DIN-EN-50113 standards [39,40]. Although they are only related to metals, in this research, the fatigue properties of magnesium alloys (with and without polymeric coatings) were studied, and the mentioned standard was utilized. The map of standard specimens is depicted in Figure 5.

**Figure 5.** The map of the fatigue standard specimen.

To perform this test, the SFT-600 device made by Santam Company was used. All experiments were conducted at room temperature and under a loading frequency of 100 Hz. Fatigue tests were performed for samples under 4 stress levels of 80, 100, 120, and 140 MPa, with a repeatability of 3 tests for each sample. The fatigue limit of magnesium was considered to be 60 MPa after 1 million cycles [41].

2.4. Fracture Surface Analysis

The fracture surfaces of the samples were seen by field-emission scanning electron microscopy (FESEM), the Sigma 300 model, made in Zeiss, Germany. Before imaging, a gold coating layer was also applied to the specimen surfaces.

3. Results and Discussion

The samples with the coating were placed in the SBF solution for 27 days. Then, the weight of the specimens was recorded during this period. Figure 6 depicts the change in weight according to the number of days that the samples were in the solution. According to this figure, the weight of the samples did not change in the first few days. However, on some days it decreased, and then, on the last few days, the weight of the sample increased. This is due to water absorption by the polymer coating [42,43]. Hasanpour et al. [44] investigated the water absorption and corrosion of pure magnesium and magnesium with PLA. The specimens were immersed in the SBF solution for 30 days. It was concluded that the corrosion rate in samples with PLA is increased due to more water absorption. Balogova et al. [45] showed that the mass of PLA samples increases with increasing water absorption. Redondo et al. [46] also reported water absorption in corrosion tests for PLA samples. Alksne et al. [47] reported swelling and water absorption over time for composite samples made of PLA + hydroxyapatite (HA) and PLA + bioglass (BG).

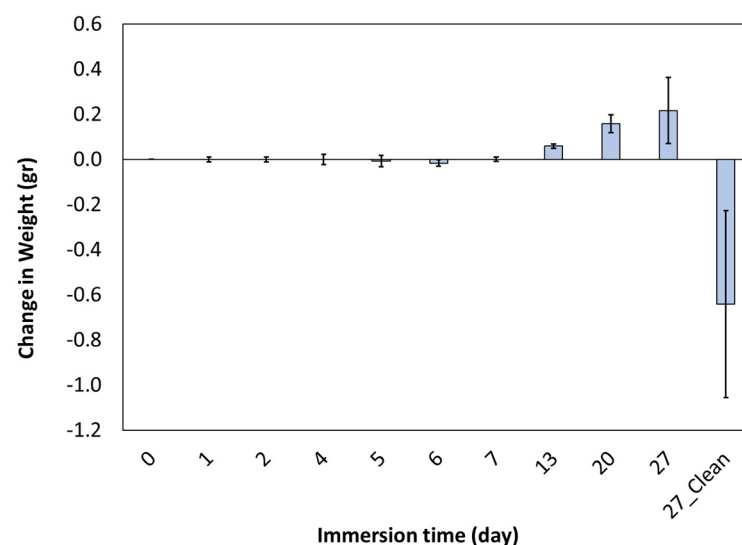


Figure 6. The changes in weight of the corroded specimens.

Figure 7 shows the corrosion rate and the average rate of corrosion. Based on this figure, the corrosion rates decreased over time. Chor et al. [48] also reported a decrease in the corrosion rate over time for a sample made of PLA materials. Voicu et al. [49] combined MgZ31 with PLA nanofibers, and the corrosion of samples in SBF solution was investigated. The results illustrated that the rate of corrosion decreased with the help of the PLA coating. Shi et al. [50] fabricated a PLA layer on the sample by placing AZ31 in the PLA-chloroform solution. The corrosion results demonstrated that the coating layers decreased the corrosion rate.

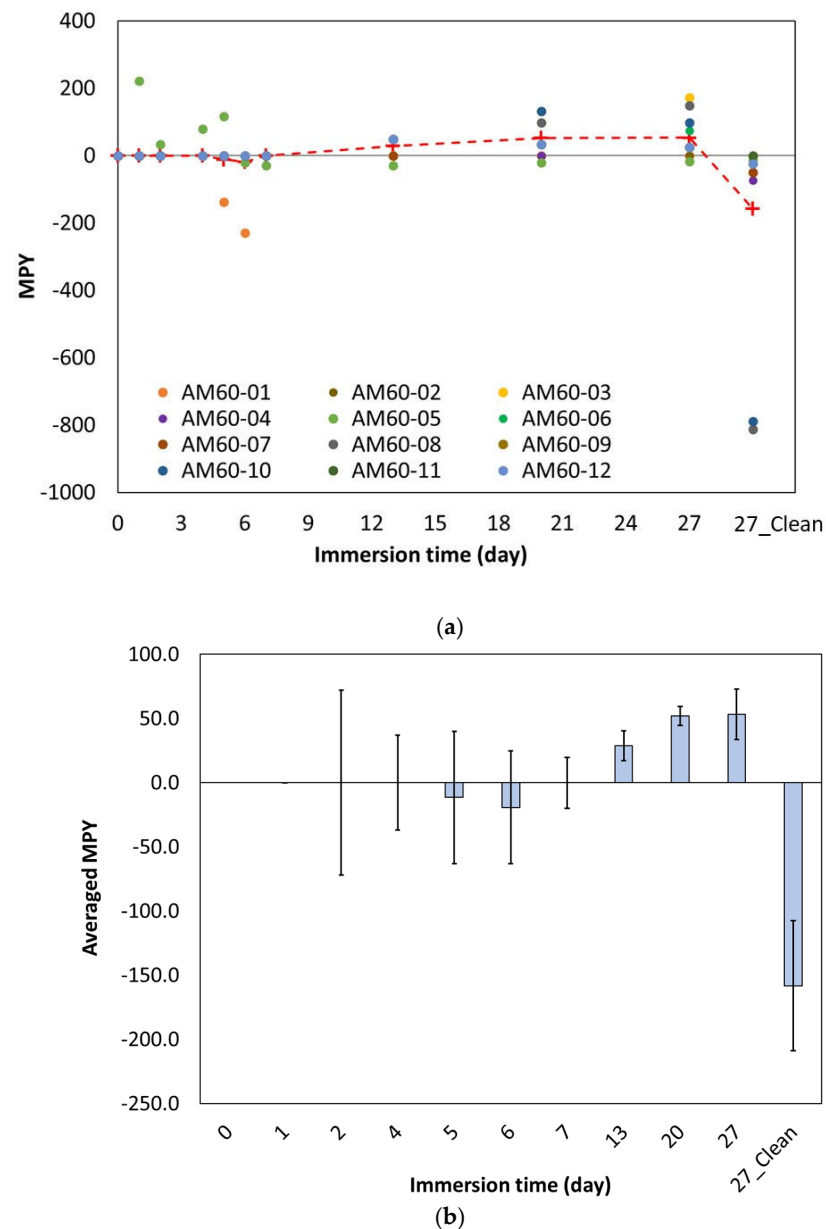


Figure 7. (a) The corrosion rate and (b) the averaged corrosion rate for coated samples.

Figure 8 shows the stress–lifetime curve for all samples and the average of samples PF-AM60-PLA and CF-AM60-PLA compared to samples PF-AM60 and CF-AM60. The Basquin formulation is shown in Equation (2) [51]. In this regard, σ'_f is the coefficient of fatigue strength, b is the exponent of fatigue strength, and N_f is the fatigue lifetime. These coefficients are reported in Table 4.

$$\sigma_a = \sigma'_f (2N_f)^b \quad (2)$$

According to Table 4, R^2 for all samples is within the acceptable range. Only in CF-AM60-PLA samples has the value of R^2 decreased. Some of these samples were highly corroded compared to similar samples. These samples are shown in Figure 8a. Because of that, their corrosion fatigue lifetime has been greatly reduced. Compared to the PF-AM60 sample, the PF-AM60-PLA sample on average had a 49% increase in fatigue lifetime. This is exactly as expected. The PLA coating has increased the cross-sectional area of the sample. Therefore, fatigue resistance has increased. However, at higher stress levels, the

fatigue lifetime increased up to 67%. The fatigue lifetime of CF-AM60-PLA specimens has decreased compared to CF-AM60 samples. However, it should be considered that the 10× SBF solution was used for CF-AM60-PLA samples. In fact, despite using a 10-times stronger solution, the fatigue lifetime decreased by only 35%.

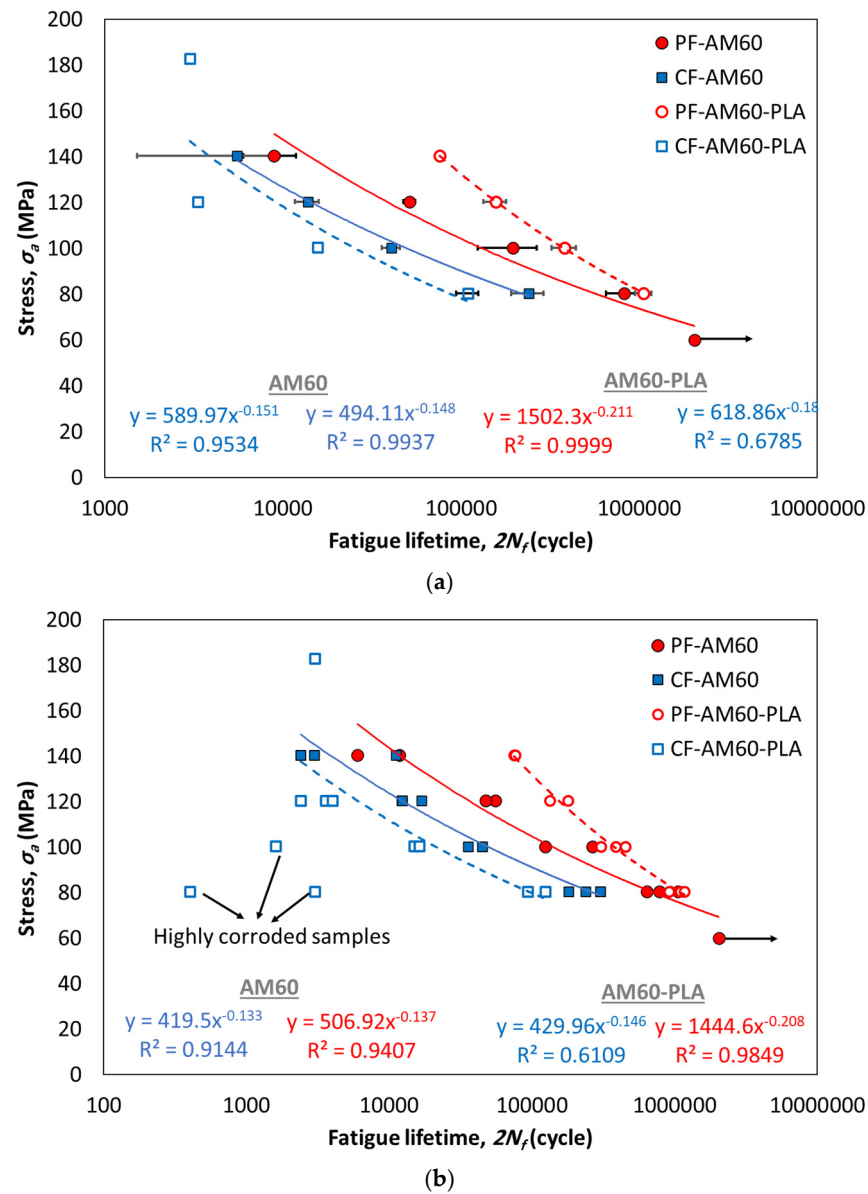


Figure 8. The stress–lifetime curves of AM60 and AM60 + PLA for (a) averaged data and (b) all data.

Table 4. The obtained fatigue properties of the AM60 magnesium alloy.

Test Conditions	All Data			Average Data		
	σ'_f (MPa)	b	R^2	σ'_f	b	R^2
PF-AM60	506.92	−0.137	0.9407	589.97	−0.151	0.9534
CF-AM60	419.50	−0.133	0.9144	494.11	−0.148	0.9999
PF-AM60-PLA	1444.60	−0.208	0.9849	1502.30	−0.211	0.9999
CF-AM60-PLA	429.96	−0.146	0.6109	618.86	−0.180	0.6785

Based on the experimental data in Figure 8, several comparisons of the obtained results could be performed with the literature for the root cause of fatigue failure. Under CF conditions, Nan et al. [52] presented that 70–80% of the fatigue lifetime was occupied due to the corrosion crack initiation. In other words, the corrosion fatigue lifetime under lower stresses was determined by the growth behavior of corrosion pits. As claimed by Bhuiyan et al. [53], this ratio of the pit growth lifetime to the fatigue crack nucleation and total fatigue lifetime was almost 30%. Notably, this crack initiation lifetime ratio must be considered with the effect of the applied stress. They claimed that most of the initiation lifetime was spent on the corrosion pit generation [53]. It must be noted that these issues may occur when fatigue testing is conducted inside the corrosive medium. However, in this study, fatigue tests were performed on the pre-corroded specimens. When the samples emerge from the SBF, the defects and pits that occur on the surface of the specimens will act as the stress concentration that boosts the crack initiation stage [54]. More transgranular or intergranular cracks can propagate under the CF condition [55].

Figure 9 shows the FESEM images of the fracture surfaces of the PF-AM60-PLA at 80 MPa of the stress level. In these figures, PLA coating and glue were seen separately. In addition, striations caused by fatigue loading were seen. Cleavage was also observed on the fracture surfaces of this specimen, which indicated the brittleness of the material [23]. In general, there are three stages containing the crack initiation, the crack growth, and the final failure due to fatigue loading. Due to bending fatigue loading, the highest stress occurs on the surface of the samples. Therefore, cracks start and grow in these areas. In the last stage, the sudden and final failure of the specimen occurs [55,56].

Figure 10 depicts the fracture surfaces of the PF-AM60-PLA at 120 MPa of the stress level. In this sample, the separation of glue and AM60 and the separation of glue and PLA coating were observed. Similarly, striations and microcracks were also seen, along with defects on the fracture surfaces of PLA coatings. These defects are spherical, and their diameter is about 0.01 mm. One of the causes of these defects was the temperature of the nozzle during 3D printing. The temperature of 180 °C for PLA causes the material to vaporize. These vapors create bubbles in the sample. After bursting, these bubbles cause the formation of defects in the sample [57,58]. Such defects may occur during the filament fabrication process, through extrusion during 3D printing, or with inappropriate speed and precision in the nozzle movement or temperature. Kuznetsov et al. [59] showed that the increase in interlayer cohesion by enhancing the nozzle diameter can explain this issue. Gonabadi et al. [60] mentioned that in 3D printed parts, the filament gaps (voids) between deposited layers were due to the variation in the layer-to-layer adhesion quality and the shrinkage during cooling. Therefore, these gas cavities or voids could be eliminated using proper parameters during 3D printing. Working on this issue to eliminate or reduce these defects could be considered for future work.

Figure 11 depicts the fracture surfaces of the CF-AM60-PLA sample at 80 MPa of the stress level. The separation of glue and sample is shown as a failure mechanism. In addition, one of the effects of corrosion is cavities and holes, which were shown in research to reduce the fatigue lifetime of the specimen due to stress concentration. These products were seen in FESEM images [54,56,61]. Moreover, microcracks were observed. These microcracks enhance the crack initiation stage in fatigue loading. In an article, it was shown that these cracks appear under CF conditions [54]. In another study, it was shown that the microcracks in the sample due to corrosion caused stress concentration and decreased the fatigue lifetime of the sample [52]. Moreover, angular cleavage plates were seen on the fracture surfaces, which indicated the brittle fracture behavior of the part. Figure 12 illustrates the results of the EDS analysis. In this figure, according to Table 3, the constituent elements of the SBF are shown.

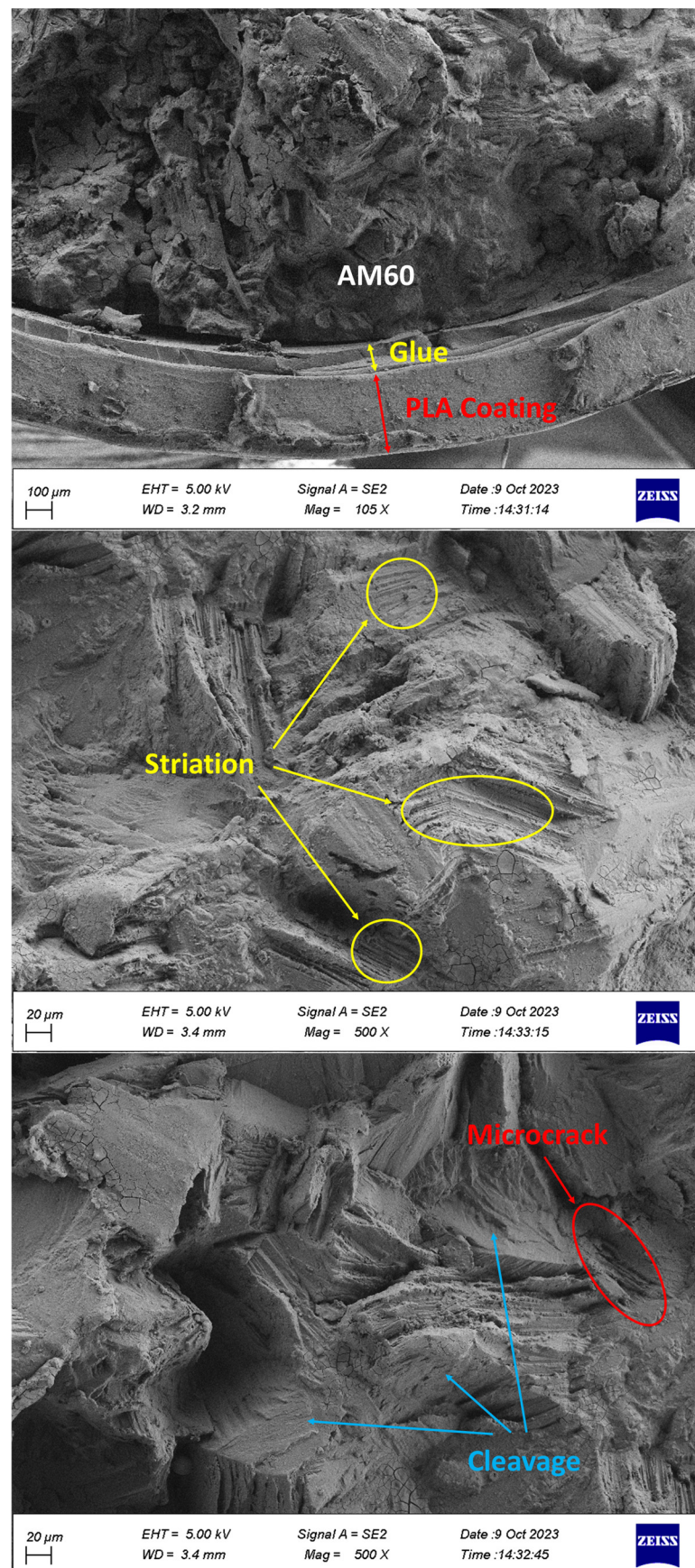


Figure 9. The fracture surface of PF-AM60-PLA at 80 MPa.

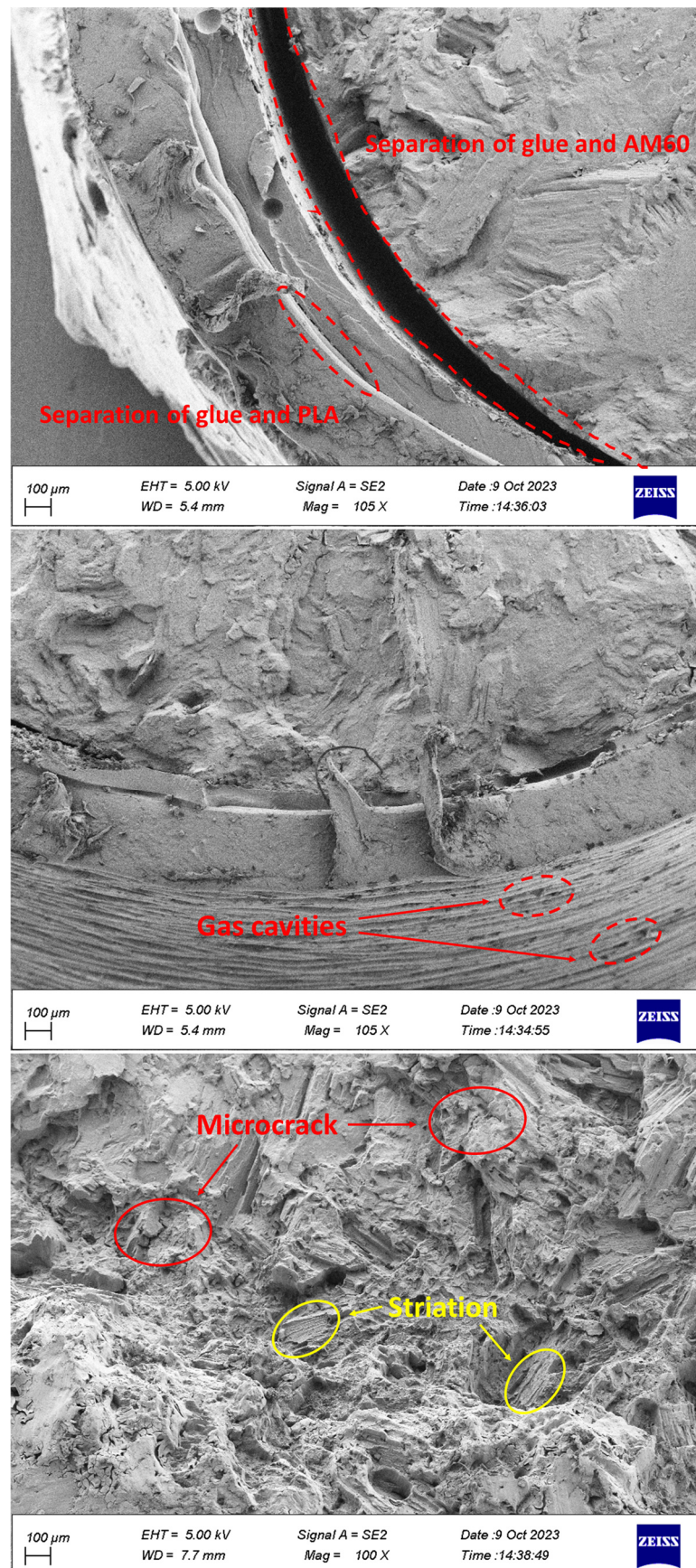


Figure 10. The fracture surface of PF-AM60-PLA at 120 MPa.

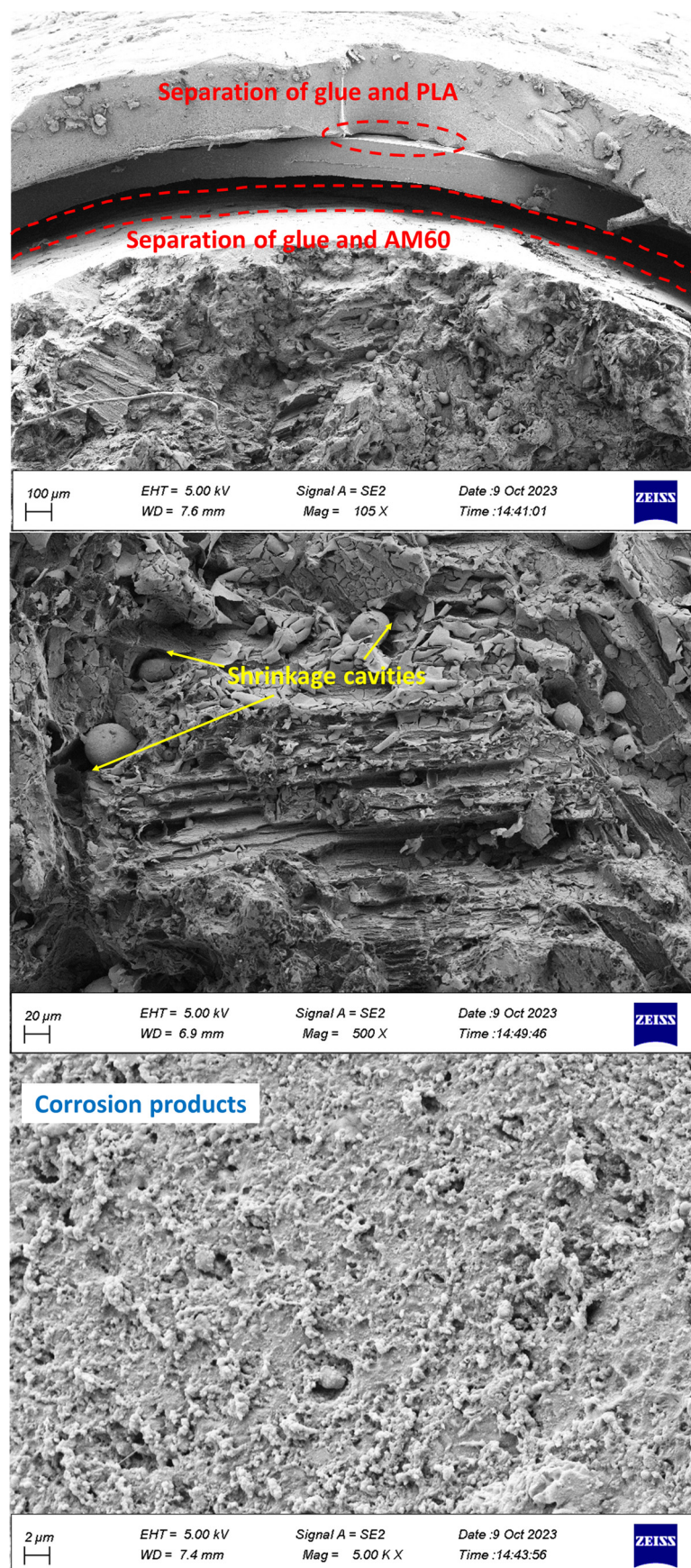


Figure 11. The fracture surface of CF-AM60-PLA at 80 MPa.

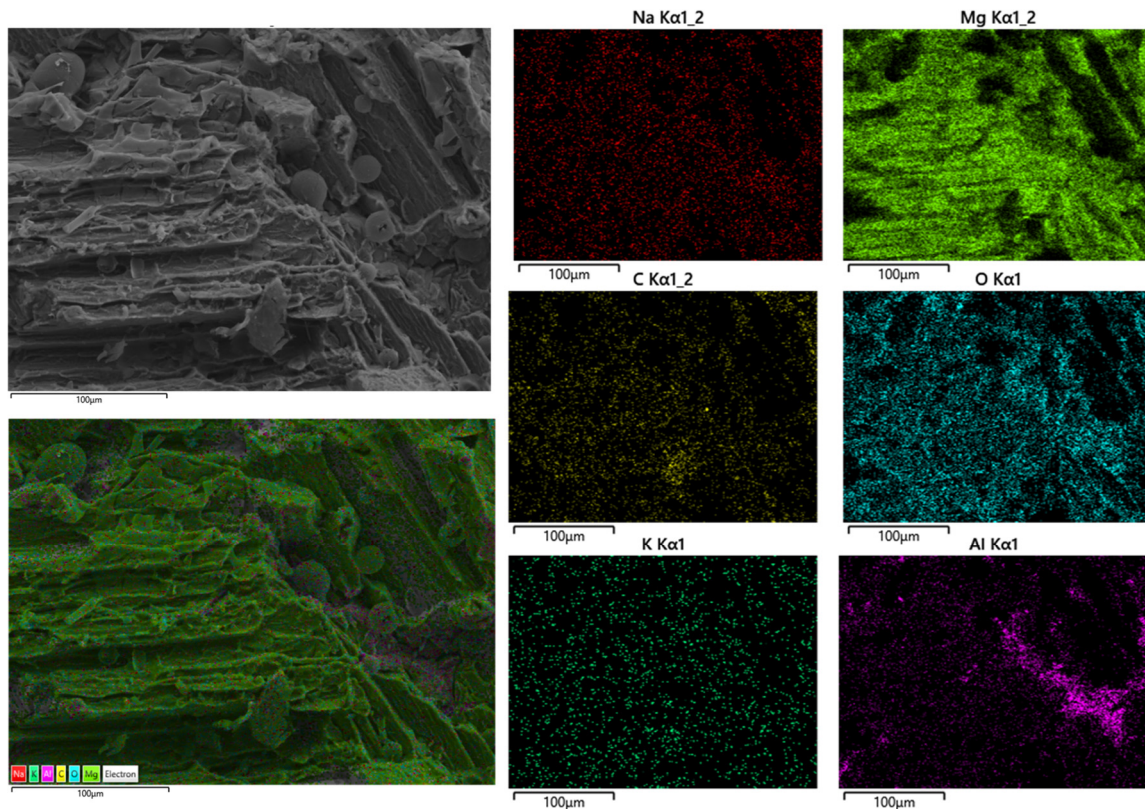


Figure 12. The EDS analysis for CF-AM60-PLA at 80 MPa.

In addition, the shrinkage holes with sphere-like particles inside the holes are also shown in Figures 11 and 12. The magnesium alloy is produced by the casting method, which is the cause of this type of shrinkage cavity. The EDS analysis demonstrated that these particles were Mg. Hu et al. [62] reported that no porosity in the AM50 magnesium alloy resulted from partial solidification of the primary α -Mg phase due to proper casting parameters such as the cooling rate during solidification. Therefore, Mg particles or intermetallics could be created by the casting process. Chen et al. [63] presented such droplets in AM60 magnesium alloys. By increasing the holding time during remelting, the intragranular liquid droplets coalesced, forming some liquid pools and migrating to the liquid matrix. These intragranular liquid droplets had two types: chemical constitution segregation and entrapping during coalescence. When the magnesium alloy is reheated above the solidus, it is possible to have several intragranular liquids form in the α -Mg matrix [63].

From the FESEM images in Figures 9–11, it could be understood that the glue thickness was between 50–150 microns. As mentioned before, it could be an uncertainty, but considering the repeatability of testing under the same condition, there is no concern about this variety. Moreover, this issue can be considered in further investigations to find the effect of the glue thickness on the strength.

Figure 13 depicts the fracture surfaces of the CF-AM60-PLA sample at 120 MPa. In this figure, the separation of glue and sample and other effects, such as cracks between the coating and the glue, are shown. In addition, shrinkage cavities were seen, indicating improper manufacturing methods, as well as cleavage plates and striations. In previous research, it was shown that the size of the holes caused by corrosion is larger in Mg alloys at higher stress levels due to the presence of Al and Zn, which leads to the initiation of cracks. Accordingly, smaller holes were created at lower levels of stress. These holes are connected, and a crack is formed [64].

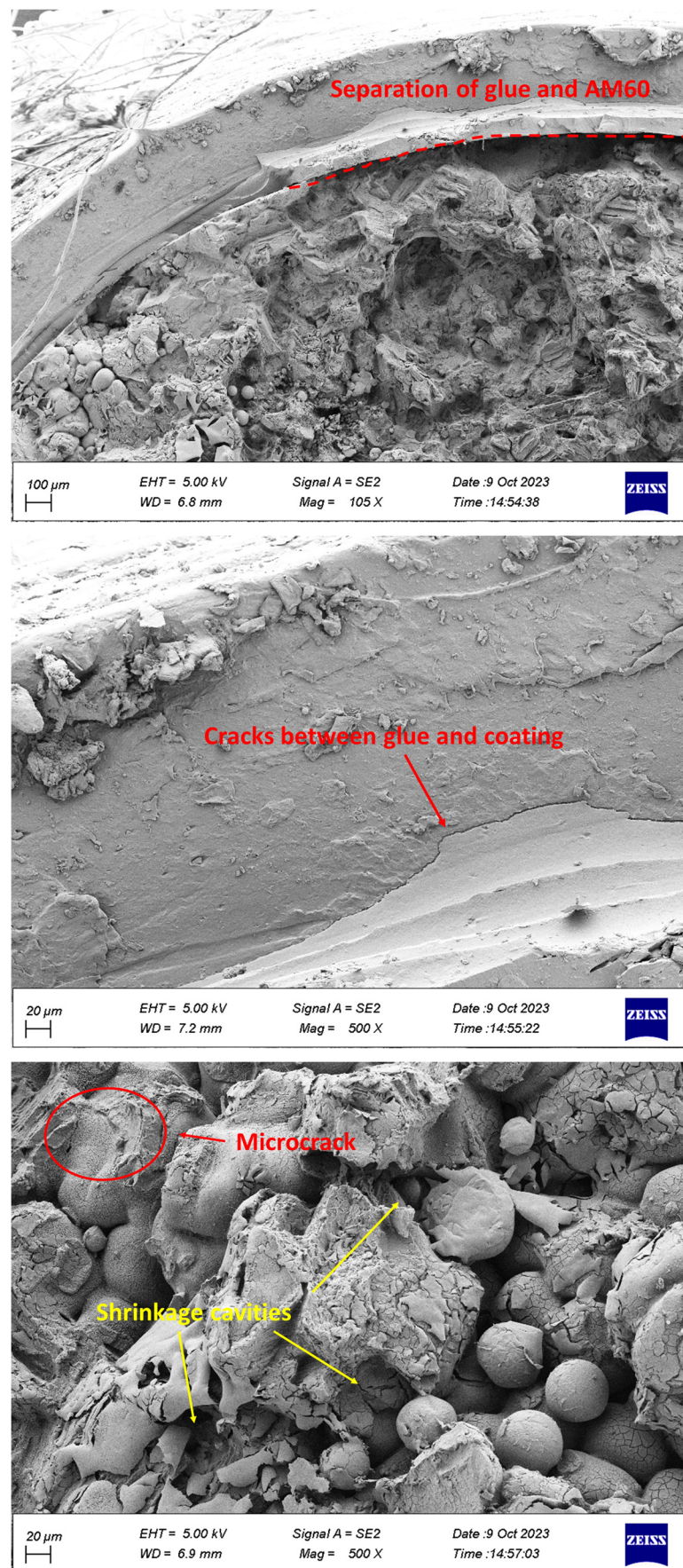


Figure 13. The fracture surface of CF-AM60-PLA at 120 MPa.

Figure 14 shows the results of the EDS analysis on the outer surface of the coating. Corrosion holes were seen on this surface. Moreover, soluble SBF elements were seen. In general, the signs of corrosion were seen only on the outer surfaces of the coating layers, and the magnesium alloy did not suffer corrosion, which is one of the advantages of using the PLA coating layers.

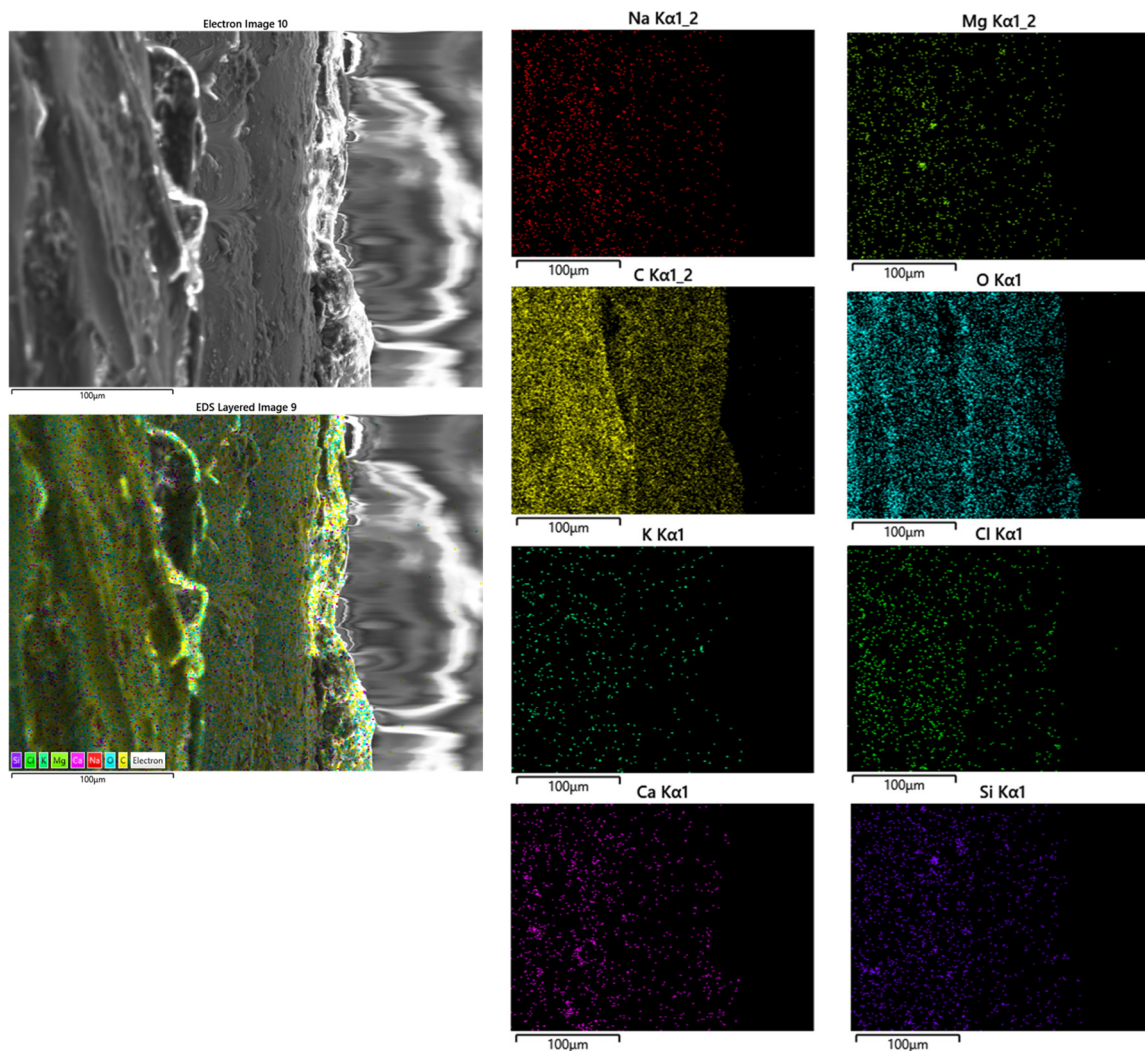


Figure 14. The EDS analysis for CF-AM60-PLA at 120 MPa.

Such an improvement in corrosion resistance with coatings was reported by Kumar [11], who used hydroxyapatite (HA) on different magnesium alloys. In another work, Uematsu et al. [20] used multilayer diamond-like carbon coatings to increase the corrosion strength of magnesium alloys under fatigue. Although these materials and their processes were different from this research (considering PLA with 3D printing), coatings on magnesium alloys have similar results in various applications, especially for biomedical engineering.

Compared to NaCl solutions in the literature [64] that have only Na and Cl elements in the NaCl medium, Figure 14 shows the presence of Ca and K elements in addition to Na and Cl elements due to the use of the SBF environment in this work. Such differences between SBF and NaCl mediums were also represented by Barzegari et al. [65], with various pH values and diffusion behaviors. Such an issue could change the corrosion behavior of the material [66], again, especially in the applications of biomedical engineering.

4. Conclusions

In the present research, the pure fatigue behaviors of magnesium alloy with polylactic acid (PLA) coating (PF-AM60-PLA) and the corrosion fatigue behaviors of magnesium alloy with PLA coating (CF-AM60-PLA) were investigated. The polymer coating was made of PLA and was made by the additive manufacturing method (3D printing). These covers were attached to the standard sample with glue. Then, the specimens were immersed in the 10× SBF for 27 days. After that, the rotary bending fatigue testing device was used to evaluate the high-cycle fatigue behaviors. Finally, the fracture surfaces of the specimens were checked with FESEM images.

Finally, the obtained experimental results show:

- Due to corrosion, the weight of the sample decreased by 35%.
- The corrosion rate decreased in the first seven days and then increased.
- Compared to the PF-AM60 sample, the PF-AM60-PLA specimen on average had a 49% increase in fatigue lifetime.
- Despite using a 10-times stronger solution, the fatigue lifetime of CF-AM60-PLA specimens is reduced by only 35% compared to CF-AM60 samples.
- The separation of coating from glue and glue from Mg was observed in the specimens.
- Cleavage plates caused by brittle fractures and striations during fatigue load were seen on the failure surface.
- Corrosion products, including microcracks and holes, were seen on the fracture surfaces of CF samples, which caused stress concentration and crack growth.
- Holes caused by the release of gases were observed in the PLA coating layers, which were fabricated by 3D printing.

Author Contributions: Conceptualization, M.A.; methodology, M.A. and S.A.A.T.; software, S.A.A.T.; validation, M.A.; formal analysis, S.A.A.T.; investigation, M.A. and S.A.A.T.; resources, M.A. and S.A.A.T.; data curation, S.A.A.T.; writing—original draft preparation, S.A.A.T.; writing—review and editing, M.A.; visualization, M.A. and S.A.A.T.; supervision, M.A.; project administration, M.A.; funding acquisition, M.A. All authors have read and agreed to the published version of the manuscript.

Funding: This research received no external funding.

Data Availability Statement: The data presented in this study are available on request from the corresponding author.

Conflicts of Interest: The authors declare no conflict of interest.

References

1. Wu, C.S.; Zhang, Z.; Cao, F.H.; Zhang, L.J.; Zhang, J.Q.; Cao, C.N. Study on the anodizing of AZ31 magnesium alloys in alkaline borate solutions. *Appl. Surf. Sci.* **2007**, *253*, 3893–3898. [[CrossRef](#)]
2. Moosbrugger, C. *Engineering Properties of Magnesium Alloys*; ASM International: Materials Park, OH, USA, 2017.
3. Zartner, P.; Cesnjevar, R.; Singer, H.; Weyand, M. First successful implantation of a bio-degradable metal stent into the left pulmonary artery of a preterm baby. *Catheter Cardiovasc. Interv.* **2005**, *66*, 590–594. [[CrossRef](#)]
4. Heublein, B.; Rohde, R.; Kaese, V.; Niemeyer, M.; Hartung, W.; Haverich, A. Bio-corrosion of magnesium alloys: A new principle in cardiovascular implant technology. *Heart* **2003**, *89*, 651–656. [[CrossRef](#)]
5. Baril, G.; Blanc, C.; Pebere, N. AC impedance spectroscopy in characterizing time-dependent corrosion of AZ91 and AM50 magnesium alloys characterization with respect to their microstructures. *J. Electrochem. Soc.* **2001**, *148*, B489. [[CrossRef](#)]
6. Staiger, M.P.; Pietak, A.M.; Huadmai, J.; Dias, G. Magnesium and its alloys as orthopedic biomaterials: A review. *Biomaterials* **2006**, *27*, 1728–1734. [[CrossRef](#)] [[PubMed](#)]
7. Song, Y.; Liu, D.; Tang, W.; Dong, K.; Shan, D.; Han, E. Comparison of the corrosion behavior of AM60 Mg alloy with and without self-healing coating in atmospheric environment. *J. Magnes. Alloys* **2021**, *9*, 1220–1232. [[CrossRef](#)]
8. Liu, W.; Cao, F.; Jia, B.; Zheng, L.; Zhang, J.; Cao, C.; Li, X. Corrosion behavior of AM60 magnesium alloys containing Ce or La under thin electrolyte layers. Part 2: Corrosion product and characterization. *Corros. Sci.* **2010**, *52*, 639–650. [[CrossRef](#)]

9. Matsubara, H.; Ichige, Y.; Fujita, K.; Nishiyama, H.; Hodouchi, K. Effect of impurity Fe on corrosion behavior of AM50 and AM60 magnesium alloys. *Corros. Sci.* **2013**, *66*, 203–210. [[CrossRef](#)]
10. Xie, Z.; Luo, Z.; Yang, Q.; Chen, T.; Tan, S.; Wang, Y.; Luo, Y. Improving anti-wear and anti-corrosion properties of AM60 magnesium alloy by ion implantation and Al/AlN/CrAlN/CrN/MoS₂ gradient duplex coating. *Vacuum* **2014**, *101*, 171–176. [[CrossRef](#)]
11. Kumar, D. Effect of hydroxyapatite (HA) addition on microstructure, corrosion resistance of AZ91D, AJ62 and AM60 alloys. *Mater. Today Proc.* **2022**, *50*, 582–584. [[CrossRef](#)]
12. Chenghao, L.; Shusen, W.; Naibao, H.; Zhihong, Z.; Shuchun, Z.; Jing, R. Effects of lanthanum and cerium mixed rare earth metal on abrasion and corrosion resistance of AM60 magnesium alloy. *Rare Met. Mater. Eng.* **2015**, *44*, 521–526. [[CrossRef](#)]
13. Ikpi, M.E.; Dong, J.; Ke, W. Electrochemical Investigation of the Galvanic Corrosion of AM60 and AD62 Magnesium Alloy in 0.1 M NaCl Solution Magdalene. *Int. J. Electrochem. Sci.* **2015**, *10*, 552–563. [[CrossRef](#)]
14. Liu, D.; Song, Y.; Shan, D.; Han, E. Comparison of the inhibition effect of four inhibitors on the corrosion behavior of AM60 magnesium alloy. *Int. J. Electrochem. Sci.* **2019**, *13*, 2219–2235. [[CrossRef](#)]
15. Jin-Ling, Z.; Yang-Li, L.; Jing, Z.; Zhi-Yong, F.; She-Bin, W. Kinetic study on the corrosion behavior of AM60 magnesium alloy with different Nd contents. *J. Alloys Compd.* **2015**, *629*, 290–296. [[CrossRef](#)]
16. Akbaripannah, F.; Fereshteh-Saniee, F.; Mahmudi, R.; Kim, H.K. The influences of extrusion and equal channel angular pressing (ECAP) processes on the fatigue behavior of AM60 magnesium alloy. *Mater. Sci. Eng. A* **2013**, *565*, 308–316. [[CrossRef](#)]
17. Khan, S.A.; Miyashita, Y.; Mutoh, Y.; Koike, T. Fatigue behavior of anodized AM60 magnesium alloy under humid environment. *Mater. Sci. Eng. A* **2008**, *498*, 377–383. [[CrossRef](#)]
18. Hiromoto, S.; Tomozawa, M.; Maruyama, N. Fatigue property of a bioabsorbable magnesium alloy with a hydroxyapatite coating formed by a chemical solution deposition. *J. Mech. Behav. Biomed. Mater.* **2013**, *25*, 1–10. [[CrossRef](#)]
19. Singh Raman, R.K.; Jafari, S.; Harandi, S.E. Corrosion fatigue fracture of magnesium alloys in bioimplant applications: A review. *Eng. Fract. Mech.* **2015**, *137*, 97–108. [[CrossRef](#)]
20. Uematsu, Y.; Kakiuchi, T.; Teratani, T.; Harada, Y.; Tokaji, K. Improvement of corrosion fatigue strength of magnesium alloy by multilayer diamond-like carbon coatings, Improvement of corrosion fatigue strength of magnesium alloy by multilayer diamond-like carbon coatings. *Surf. Coat. Technol.* **2011**, *205*, 2778–2784. [[CrossRef](#)]
21. AlamKhan, S.; Bhuiyan, M.S.; Miyashita, Y.; Mutoh, Y.; Koike, T. Corrosion fatigue behavior of die-cast and shot-blasted AM60 magnesium alloy. *Mater. Sci. Eng. A* **2011**, *528*, 1961–1966. [[CrossRef](#)]
22. Ishihara, S.; Namito, T.; Notoya, H.; Okada, A. The corrosion fatigue resistance of an electrolytically-plated magnesium alloy. *Int. J. Fatigue* **2010**, *32*, 1299–1305. [[CrossRef](#)]
23. Talesh, S.A.A.; Azadi, M. High-cycle fatigue testing on AM60 magnesium alloy samples for as-received and pre-corroded conditions in simulated body fluid. *J. Mater. Res. Technol.* **2023**, *27*, 1922–1934. [[CrossRef](#)]
24. Antunes, R.A.; De Oliveira, M.C.L. Corrosion fatigue of biomedical metallic alloys: Mechanisms and mitigation. *Acta Biomater.* **2012**, *8*, 937–962. [[CrossRef](#)] [[PubMed](#)]
25. Delavar, H.; Mostahsan, A.J.; Ibrahim, H. Corrosion and corrosion-fatigue behavior of magnesium metal matrix composites for bio-implant applications: A review. *J. Magnes. Alloys* **2023**, *11*, 1125–1161. [[CrossRef](#)]
26. Shi, Y.; Yang, L.; Zhang, Q.; Zhu, X.; Song, Z.; Liu, H. A novel MAO-PLA coating on zinc alloy for potential orthopedic implant material. *Mater. Lett.* **2022**, *317*, 132058. [[CrossRef](#)]
27. Anand, N.; Pal, K. Evaluation of biodegradable Zn-1Mg-1Mn and Zn-1Mg-1Mn-1HA composites with a polymer-ceramics coating of PLA/HA/TiO₂ for orthopaedic applications. *J. Mech. Behav. Biomed. Mater.* **2022**, *136*, 105470. [[CrossRef](#)]
28. Wang, A.; Venezuela, J.; Dargusch, M.S. Enhancing the corrodibility of biodegradable iron and zinc using poly (lactic) acid (PLA) coating for temporary medical implant applications. *Prog. Org. Coat. J.* **2023**, *174*, 107301. [[CrossRef](#)]
29. Beyzavi, A.H.; Azadi, M.; Azadi, M.; Dezianian, S.; Talebsafa, V. Bio-polymer coatings fabricated on AM60 magnesium alloys by fused deposition modeling 3D-printing to investigate electrochemical behavior. *Mater. Lett.* **2023**, *337*, 133935. [[CrossRef](#)]
30. Rezanezhad, S.; Azadi, M. Amazing epsilon-shaped trend for fretting fatigue characteristics in AM60 magnesium alloy under stress-controlled cyclic conditions at bending loads with zero mean stress. *PLoS ONE* **2023**, *18*, 0281263. [[CrossRef](#)]
31. Dezianian, S.; Azadi, M. Multi-material metamaterial topology optimization to minimize the compliance and the constraint of weight: Application of non-pneumatic tire additive-manufactured with PLA/TPU polymers. *Polymers* **2023**, *15*, 1927. [[CrossRef](#)]
32. Dezianian, S.; Azadi, M.; Razavi, S.M.J. Topology optimization on metamaterial cells for replacement possibility in non-pneumatic tire and the capability of 3D-printing. *PLoS ONE* **2023**, *18*, e0290345. [[CrossRef](#)] [[PubMed](#)]
33. Rezanezhad, S.; Azadi, M. Impact of 3D-printed PLA coatings on the mechanical and adhesion properties of AM60 magnesium alloys. *Compos. Part C* **2023**, *12*, 100415. [[CrossRef](#)]
34. Azadi, M.; Dadashi, A.; Dezianian, S.; Kianifar, M.; Torkaman, S.; Chiyani, M. High-cycle bending fatigue properties of additive-manufactured ABS and PLA polymers fabricated by fused deposition modeling 3D-printing. *Forces Mech.* **2021**, *3*, 100016. [[CrossRef](#)]
35. Rudawska, A.; Sarna-Bos, K.; Rudawska, A.; Rozylo-Kalinowska, I.; Chalas, R. Biological and chemical properties of cured epoxy resins. *Res. Sq.* **2021**. [[CrossRef](#)]

36. Munoz, M.; Torres, B.; Mohedano, M.; Matykina, E.; Arrabal, R.; Lopez, A.J.; Rams, J. PLA deposition on surface treated magnesium alloy: Adhesion, toughness and corrosion behavior. *Surf. Coat. Technol.* **2020**, *388*, 125593. [[CrossRef](#)]
37. *Simulated Body Fluid Catalog*; Pardis Pajouhesh Fanavaran Yazd Company, Yazd Science and Technology Park: Yazd, Iran, 2023.
38. ASTM G31-72; Standard Practice for Laboratory Immersion Corrosion Testing of Metals. ASTM International: West Conshohocken, PA, USA, 2004.
39. ISO 1143:2010; Metallic Materials—Rotating Bar Bending Fatigue Testing. International Organization for Standardization: Geneva, Switzerland, 2010.
40. DIN EN 50113; Rotating Bar Bending Fatigue Test. DIN Standard: Berlin, Germany, 1982.
41. Oliya, A.Y.P.; Azadi, M.; Parast, M.S.A.; Mokhtarishirazabad, M. Effect of heat-treating on microstructure and high cycle bending fatigue behavior of AZ91 and AZE911 magnesium alloys. *Adv. Mater. Sci. Eng.* **2022**, *2022*, 4030062. [[CrossRef](#)]
42. Hodaieian, H. Degradation of Pure Magnesium Alloys in Simulated Body Fluid. Master's Thesis, University of Birmingham, Birmingham, UK, 2013.
43. Guo, Z.; Yang, C.; Zhou, Z.; Chen, S.; Li, F. Characterization of biodegradable poly (lactic acid) porous scaffolds prepared using selective enzymatic degradation for tissue engineering. *R. Soc. Chem. Adv.* **2017**, *7*, 34063. [[CrossRef](#)]
44. Hasanpur, E.; Ghazavizadeh, A.; Sadeghi, A.; Haboussi, M. In vitro corrosion study of PLA/Mg composites for cardiovascular stent applications. *J. Mech. Behav. Biomed. Mater.* **2021**, *124*, 104768. [[CrossRef](#)]
45. Balogova, A.; Trebunova, M.; Izarikova, G.; Kascak, L.; Mitrik, L.; Klimova, J.; Feranc, J.; Modrak, M.; Hudak, R.; Zivcak, J. In vitro degradation of specimens produced from PLA/PHB by additive manufacturing in simulated conditions. *Polymers* **2021**, *13*, 1542. [[CrossRef](#)]
46. Redondo, F.; Giaroli, M.; Ciolino, A.; Ninago, M. Preparation of Porous Poly (Lactic Acid)/Tricalcium Phosphate Composite Scaffolds for Tissue Engineering. *Biointerface Res. Appl. Chem.* **2022**, *12*, 5610–5624.
47. Alksne, M.; Kalvaityte, M.; Simoliunas, E.; Rinkunaite, I.; Gendviliene, I.; Locs, J.; Rutkunas, V.; Bukelskiene, V. In vitro comparison of 3D printed polylactic acid/hydroxyapatite and polylactic acid/bio-glass composite scaffolds: Insights into materials for bone regeneration. *J. Mech. Behav. Biomed. Mater.* **2020**, *104*, 103641. [[CrossRef](#)]
48. Chor, A.; Gonçalves, R.; Costa, A.; Farina, M.; Ponche, A.; Sirelli, L.; Schrodj, G.; Gree, S.; Andrade, L.; Anselme, K.; et al. In vitro degradation of electro-spun poly (lactic-Co-glycolic acid) (PLGA) for oral mucosa regeneration. *Polymers* **2020**, *12*, 1853. [[CrossRef](#)]
49. Voicu, M.E.; Demetrescu, I.; Dorobantu, A.; Enachescu, M.; Buica, G.O.; Ionita, D. Interaction of Mg alloy with PLA electro-spun nanofibers coating in understanding changes of corrosion. *Nanomaterials* **2022**, *12*, 12081369. [[CrossRef](#)]
50. Shi, P.; Niu, B.; Shanshan, E.; Chen, Y.; Li, Q. Preparation and characterization of PLA coating and PLA/MAO composite coatings on AZ31 magnesium alloy for improvement of corrosion resistance. *Surf. Coat. Technol.* **2015**, *262*, 26–32. [[CrossRef](#)]
51. Basquin, O.H. The exponential law of endurance tests. *Proc. Am. Soc. Test. Mater.* **1910**, *10*, 625–630.
52. Nan, Z.Y.; Ishihara, S.; Goshima, T. Corrosion fatigue behavior of extruded magnesium alloy AZ31 in sodium chloride solution. *Int. J. Fatigue* **2008**, *30*, 1181–1188. [[CrossRef](#)]
53. Bhuiyan, M.S.; Mutoh, Y.; Murai, T.; Iwakami, S. Corrosion fatigue behavior of extruded magnesium alloy AZ61 under three different corrosive environments. *Int. J. Fatigue* **2008**, *30*, 1756–1765. [[CrossRef](#)]
54. Parast, M.S.A.; Azadi, M. A short evaluation of simultaneous corrosion fretting fatigue behaviors in piston aluminum-silicon alloys considering effects of nano-particles and heat-treating. *Int. J. Fatigue* **2023**, *168*, 107403. [[CrossRef](#)]
55. Stephens, R.; Fatemi, A.; Stephens, R.; Fuchs, H. *Metal Fatigue in Engineering*; John Wiley and Sons: Hoboken, NJ, USA, 2000.
56. Ghazizadeh, E.; Jabbari, A.H.; Sedighi, M. In vitro corrosion fatigue behavior of biodegradable Mg/HA composite in simulated body fluid. *J. Magnes. Alloys* **2021**, *9*, 2169–2184. [[CrossRef](#)]
57. Mokhtarishirazabad, M.; Azadi, M.; Farrahi, G.H.; Winter, G.; Eichlseder, W. Improvement of high temperature fatigue lifetime in AZ91 magnesium alloy by heat treatment. *Mater. Sci. Eng. A* **2013**, *588*, 357–365. [[CrossRef](#)]
58. Jiang, L.; Xu, F.; Xu, Z.; Chen, Y.; Zhou, X.; Wei, G.; Ge, H. Biodegradation of AZ31 and WE43 magnesium alloys in simulated body fluid. *Int. J. Electrochem. Sci.* **2015**, *10*, 10422–10432. [[CrossRef](#)]
59. Kuznetsov, V.E.; Solonin, A.N.; Urzhumtsev, O.D.; Schilling, R.; Tavitov, A.G. Strength of PLA components fabricated with fused deposition technology using a desktop 3D printer as a function of geometrical parameters of the process. *Polymers* **2018**, *10*, 313. [[CrossRef](#)]
60. Gonabadi, H.; Yadav, A.; Bull, S.J. The effect of processing parameters on the mechanical characteristics of PLA produced by a 3D FFF printer. *Int. J. Adv. Manuf. Technol.* **2020**, *111*, 695–709. [[CrossRef](#)]
61. Liu, M.; Wang, J.; Zhu, S.; Zhang, Y.; Sun, Y.; Wang, L.; Guan, S. Corrosion fatigue of the extruded Mg-Zn-Y-Nd alloy in simulated body fluid. *J. Magnes. Alloys* **2020**, *8*, 231–240. [[CrossRef](#)]
62. Hu, H.; Zhou, M.; Sun, Z.; Li, N. Tensile behavior and fracture characteristics of die cast magnesium alloy AM50. *J. Mater. Process. Technol.* **2008**, *201*, 364–368. [[CrossRef](#)]
63. Chen, Q.; Zhao, Z.; Chen, G.; Wang, B. Effect of accumulative plastic deformation on generation of spheroidal structure, thixoforability and mechanical properties of large-size AM60 magnesium alloy. *J. Alloys Compd.* **2015**, *632*, 190–200. [[CrossRef](#)]
64. Bhuiyan, M.S.; Mutoh, Y.; Murai, T.; Iwakami, S. Corrosion fatigue behavior of extruded magnesium alloy AZ80-T5 in a 5% NaCl environment. *Eng. Fract. Mech.* **2010**, *77*, 1567–1576. [[CrossRef](#)]

-
65. Barzegari, M.; Mei, D.; Lamaka, S.V.; Geris, L. Computational modeling of degradation process of biodegradable magnesium biomaterials. *Corros. Sci.* **2021**, *190*, 109674. [[CrossRef](#)]
 66. Mei, D.; Lamaka, S.V.; Lu, X.; Zheludkevich, M.L. Selecting medium for corrosion testing of bioabsorbable magnesium and other metals—A critical review. *Corros. Sci.* **2020**, *171*, 108722. [[CrossRef](#)]

Disclaimer/Publisher’s Note: The statements, opinions and data contained in all publications are solely those of the individual author(s) and contributor(s) and not of MDPI and/or the editor(s). MDPI and/or the editor(s) disclaim responsibility for any injury to people or property resulting from any ideas, methods, instructions or products referred to in the content.